한국가시화정보학회지, 제6권, 제1호, (2008) 3~16
<특집기사>

교류 전기삼투유동 - 근본 메커니즘과 운동학적 양상

서용권†

AC-Electroosmotic Flows-Fundamental Mechanism and Kinematic Aspects

Yonk Kweon Suh†

Abstract. Controlling fluid flows in micro scales is a non-trivial issue among those who are involved in designing lab-on-chips. Pumping and mixing by using electrokinetic principles has been popular in that the method requires a few parts and it is easy to control. This paper explains the basic mechanism of the electroosmotic flows caused by AC together with presenting some numerical results. In particular, the fundamental, physical idea involved in the mechanism will be illustrated in terms of the kinematic aspect. Since the electroosmotic flows are mainly driven by the motion of ions, we also demonstrate the ion motions by using the numerical-visualization method.

Key Words: Kinematics(운동학), Ion transport(이온수송), Electroosmotic flow(전기삼투 유동), Numerical visualization(수치가시화)

1. Introduction

Recently there has been great interest in applying electrokinetic forces in controlling microfluidic flows, e.g. to pump a liquid and/or to achieve good mixing. While the DC forcing is adequate for globally pumping liquid inside a rather long channel having a certain amount of wall charge, the AC forcing is suitable for generating local flows so that it can be more useful in controlling fluid flows without so much affecting the global flows. AC electroosmotic flows are generated by applying AC to a pair of electrodes patterned usually on a coplanar wall with a small gap, typically 20 micrometers. As in the DC electroosmotic flows, the fundamental force that drives the fluid flows with the AC flows comes from the charge caused by the non-equilibrium ion distribution near the electrodes.

The Helmholtz formula predicts that the magnitude of the slip velocity of the electroosmotic flows is proportional to the zeta potential and the external electric field(e.g. [1-3]); here the external electric field means the electric field outside the electric double layer (EDL). In the conventional DC electroosmotic flows, no electrodes are needed to be built inside the channel, because the channel surface has tendency to be negatively charged and thus automatically collect more cations than anions within the EDL. The net effect is to create the non-zero zeta potential across the EDL. Applying DC electric field in the tangential direction (exactly corresponding to the external electric field used in the Helmholtz formula) then causes the cations to move toward the cathode, thereby driving the whole liquid in the same direction through the viscous action; this is the so called (DC) electroosmotic flow.

On the other hand, the AC electroosmotic flows are usually created by non-equilibrium accumulation of ions around a pair of electrodes having a small gap. If the DC were applied across the electrode pair, then cations and anions would accumulate so quickly around the cathode and anode, respectively. This then screens the electrodes completely, if no Faradaic reaction were assumed to

†동아대학교 기계공학과
E-mail: yksuh@dau.ac.kr

occur (complete polarization). Therefore the external electric field vanishes and so fluid flows are not expected to occur. However when the AC is applied with a suitable level of frequency such that one period of the AC forcing is not so long as to allow the ions completely screen the electrodes, non-zero electric field is produced outside the EDL together with a certain finite amount of the zeta potential. Therefore we can expect that this should generate fluid flow along the electrode surface. When the sign of the AC potential is changed during one period of forcing, then both the zeta potential and external electric field change signs simultaneously so that the flow direction is unchanged. This is enough to understand why a steady flow velocity occurs around the electrodes when the AC is applied.

In the followings the fundamental mechanism of the fluid flows, i.e. ion transport, will be addressed with more basic terminologies especially for those who are more specialized in the fluid mechanics than in the electrochemistry. Later, some recent findings and numerical methods are introduced that can be used in calculating the slip velocity for the AC electroosmosis. Finally, the kinematic aspects of the ion motions are touched in order to provide them with further understanding of the phenomenon.

2. Ion Transport and Mass Conservation

Electroosmotic flows are driven by the motion of ions. Therefore investigating the ion transport caused by the diffusion, conduction and convection is prerequisite in order to understand the electroosmotic flows. Furthermore since the Reynolds number is very small in microfluidics, the ion motions are decoupled from the motions of the surrounding fluid. In this section we show the derivation of the Nernst-Planck equation from the principle of mass conservation, which governs the ion transport. Before that, we treat three basic mechanisms for the ion transport; diffusion, conduction and convection. More systematic touch of these topics may be found in literatures [1-4].

2.1. Diffusion

Let c_i be the concentration of an ion species i, more specifically the number density (number of ions per unit volume) [1/m^3]. Non-uniform distribution of ion concentrations leads to diffusion. Let $\mathbf{J}_i^D$ [1/m^{2}s] be the flux (number of ions passing through a surface per unit area per unit time) along the direction of $-\nabla c_i$ caused by the diffusion process, see Fig. 1. Then the Fick's 1st law states that

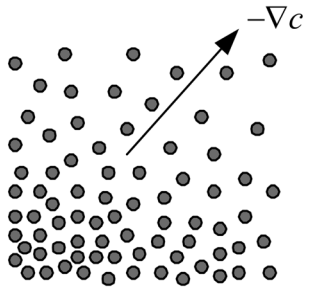

Fig. 1. Schematic of the diffusive ion-transport caused by a concentration gradient.

$$\mathbf{J}_i^D = -D_i \nabla c_i , \tag{1}$$

where D_i [m^2/s] is the diffusion coefficient or diffusivity. Stokes-Einstein equation relates D and the dynamic viscosity of the medium η [Ns/m^2] as follows.

$$D = \frac{k_B T}{6\pi a \eta}, \tag{2}$$

where k_B is the Boltzmann constant [J/K], T the temperature [K] and a the ionic radius [m].

2.2. Conduction

Conduction is the transport of ions under the influence of an electric field. The driving force for the conduction is electric field (see Fig. 2)

$$\mathbf{E} = -\nabla \phi , \tag{3}$$

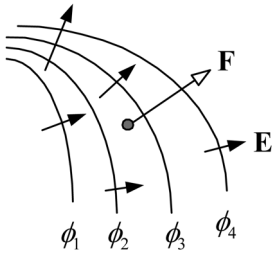

Fig. 2. Electrostatic force acting on a cation causing the conduction.

where ϕ is the potential [V]. An ion of valence z_i has the charge $z_i e$ and so the electrostatic force acted by the electric field on the ion is

$$\mathbf{F}=z_i e\mathbf{E} \text{ [N]} \tag{4}$$

where e=1.602×10^{-19} [C] is the electron charge. For the case of dilute electrolyte, this force may give rise to the ion's constant velocity relative to the surrounding medium. Assume a stationary state of the surrounding fluid, then we can set the ion's velocity $\mathbf{v}_i$ in proportion of the force **F** or the electric field **E**;

$$\mathbf{v}_i=u_i\mathbf{E} \text{ [m/s]} \tag{5}$$

where u is called 'mobility' [m^2/Vs]. Nernst-Einstein equation relates the mobility u and the diffusivity D;

$$u = \frac{|z|FD}{RT} \tag{6}$$

where $F=N_A e$=96485 [C/mol] is the Faraday constant, R=8.31 [J/mol K] the gas constant and N_A=6.02×10^{23} [1/mol] the Avogadro number. For ions large enough, we can use the Stokes' resistance law as follows.

$$u = \frac{|z|e}{6\pi\eta a} \tag{7}$$

The conductive flux of the ions of specifies i is then

$$\mathbf{J}_i^C = c_i\mathbf{v}_i = u_i c_i\mathbf{E} = D_i\left(\frac{z_i e}{k_B T}\right)c_i\mathbf{E} = -D_i\left(\frac{z_i e}{k_B T}\right)c_i\nabla\phi \tag{8}$$

where the relation $R=k_B N_A$ has been used. Conduction is sometimes called 'ion migration' [2].

2.3. Advection

The ions are also advected by the surrounding fluid's motion (Fig. 3) though this effect can be safely neglected in most cases. The transport given by the advection effect can be written in terms of the flux $\mathbf{J}_i^A$ as follows.

$$\mathbf{J}_i^A = c_i\mathbf{u} \tag{9}$$

where **u** is the velocity of the fluid.

2.4. Nernst-Planck Equation

This equation is nothing more than the conservation of the species. Assuming no chemical reaction among the specifies, we can say that the total number of ions within a system is conserved. We consider a stationary control volume V as shown in Fig. 4. The total number of ions of specifies i within this volume will be

$$\int_V c_i dV$$

The time rate of change of the ion numbers in this volume, i.e.

$$\int_V \frac{\partial c_i}{\partial t} dV$$

should be the same as the time rate of change of the number of ions, per unit time, entering through the whole control surface A surrounding the volume. So, we can write

$$\int_V \frac{\partial c_i}{\partial t} dV = -\int_A \mathbf{J}_i d\mathbf{A} = -\int_V \nabla\cdot\mathbf{J}_i dV$$

where the second equality comes from the divergence theorem, and $\mathbf{J}_i$ represents the total flux given by

$$\mathbf{J}_i = \mathbf{J}_i^D + \mathbf{J}_i^C + \mathbf{J}_i^A \tag{10}$$

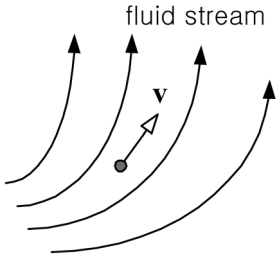

Fig. 3. Advective (or convective) transport caused by the surrounding fluid flow.

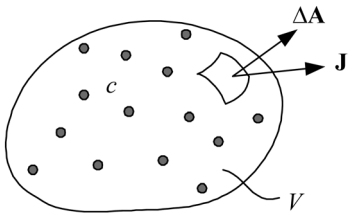

Fig. 4. Stationary control volume V with the ion concentration c inside and the total flux **J** through the surface.

Since the control volume can take an arbitrary shape and size, we must require

$$\frac{\partial c_i}{\partial t} + \nabla \cdot \mathbf{J}_i = 0 \tag{11}$$

Substituting the formula for $\mathbf{J}_i^D$, $\mathbf{J}_i^C$ and $\mathbf{J}_i^A$ into this yields

$$\frac{\partial c_i}{\partial t} + \mathbf{u}\nabla c_i = \nabla \cdot \left[D_i \nabla c_i + D_i \left(\frac{z_i e}{k_B T} \right) c_i \nabla \phi \right] \tag{12}$$

where the fluid's incompressibility was applied. This is called 'Nernst-Planck equation'.

We also use the term 'current density' $\mathbf{j}_i$ [C/m^{2}s]. This is related to the ion flux $\mathbf{J}_i$ by

$$\mathbf{j}_i = z_i e \mathbf{J}_i$$

3. Induced Electric Potential

There are two kinds of electric field, as illustrated in Fig. 5. The first one is the external electric field which is not disturbed by the presence of unbalanced distribution of ions near the surface.

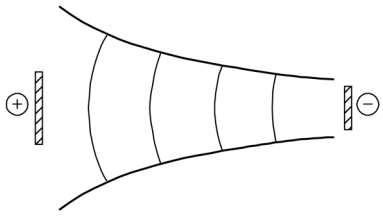

(a) external electric field

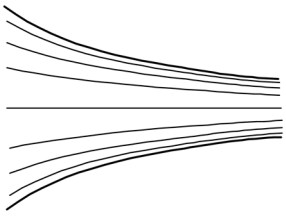

(b) induced electric field

Fig. 5. Two kinds of the electric field built inside a converging channel; (a) the electric field given externally by the difference of potentials applied at electrodes upstream and downstream ends and (b) the one induced by the non-equilibrium distribution of ions in the EDL near the channel wall.

The second one is the potential induced by the unbalanced ion-distribution. These two potentials do not directly influence each other. The induced potential ϕ is determined from the Poisson equation [3]

$$\nabla \cdot (\varepsilon \varepsilon_0 \nabla \phi) = -\rho_e \tag{13}$$

where ρ_e [C/m^3] is the local volume density of the net charge;

$$\rho_e = \sum_i z_i c_i e \tag{14}$$

Here ε_0=8.85×10^{-12} [C/Vm] is the dielectric permittivity of the vacuum and ε the relative permittivity (dimensionless) of the fluid.

4. Navier-Stokes Equations with Electric Force

Consider again a stationary control volume *V*. When the electric field **E**, internal or external, applies on this volume, each of the ions within the volume will receive the body force $z_i e\mathbf{E}$. This force then tends to move the ion in the direction of **E** and subsequently the ion drives the surrounding fluid, see Fig. 6. The fluid's driven velocity may decrease with the distance from the location of the ion. Describing such induced velocity field for each ion and considering the effect from all of the ions in estimation of the fluid velocity is almost impossible. Instead of this, we employ the momentum principle.

Assuming that within an infinitesimal volume δV there are still large number of ions, we can say that

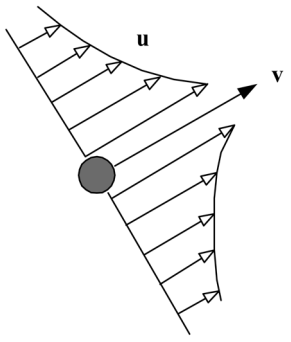

Fig. 6. Velocity profile of the surrounding fluid driven by the ion's motion.

the electric body force acting on δV is $c_i z_i e\mathbf{E}\delta V$. So, the electric body force per unit volume is simply $c_i z_i e\mathbf{E}$. We must consider contributions from all the species. Then we have

$$\rho\left(\frac{\partial \mathbf{u}}{\partial t}+\mathbf{u}\cdot\nabla\mathbf{u}\right) = -\nabla p+\eta\nabla^2\mathbf{u}-\rho_e\nabla\phi \tag{15}$$

where the ρ [kg/m^3] is the fluid density and p [N/m^2] the pressure. The continuity equation for the incompressible fluid reads

$$\nabla\cdot\mathbf{u} = 0 \tag{16}$$

In summary, we have Eqs. (12), (13), (15) and (16) for the unknowns c_i, ϕ, $\mathbf{u}$ and p. In micro scales, since the geometric scale of the flow is very small, the convective terms, i.e. the second terms in LHS of (12) and (15) can be neglected in most cases. Then the problem of the ion transport is decoupled from that of the momentum transport. So, in order to find the velocity field of the electroosmotic flow, the ion-transport equation (12) coupled with the potential equation (13) is first solved, and then the slip velocity given by the potential solution is used as the boundary condition while solving the momentum equation (15) with the continuity equation (16).

5. Electrical Thin Layers

5.1. Electric Double Layer (EDL)

When an electrolyte is in contact with a charged surface of a dielectric material, such as the colloid particle and the electrode with DC without chemical reaction, the surface attracts the counter-ions and repels the co-ions resulting in the unbalanced distribution of cations and anions in the thin layer adjacent to the interface. This layer is called diffuse layer. Thickness of the diffuse layer is dependent on the ion concentration but remains at most $O(100)$ [nm] for clean water. Because of the unbalanced ion-distribution, the electric potential difference, called 'zeta potential', exists across the diffuse layer. On the other hand, we should notice that there is a thinner layer, called 'Stern layer' or 'compact layer', between the diffuse layer and the solid surface (Fig. 7). The Stern layer is thought to be devoid of ions [3]. These two layers constitute the electric double layer.

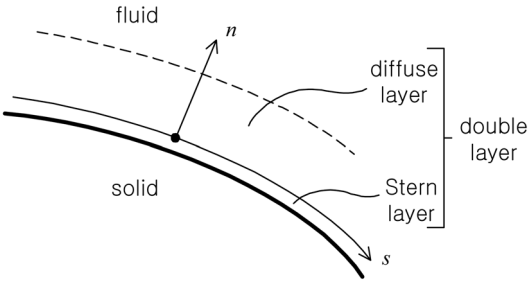

Fig. 7. Double-layer structure and the body-fitted coordinates (s,n).

Using the coordinates (s,n) for symmetric ions ($z_1=-z_2=z>0$), we can write (13) as follows.

$$\frac{\partial}{\partial n}\left(\varepsilon\varepsilon_0\frac{\partial\phi}{\partial n}\right) = -\rho_e = -ze(c^+-c^-) \tag{17}$$

where the terms containing derivative w.r.t. s have been neglected, and $c^\pm$ stand for c_1 and c_2, respectively. On the other hand, within the thin layer, the time scale concerned with the ion transport is very small. Then (12) reduces to

$$\frac{\partial c^\pm}{\partial n}\pm\frac{ze}{k_BT}c^\pm\frac{\partial\phi}{\partial n} = 0 \tag{18}$$

This is simply the balance between the diffusion and conduction terms. We can readily integrate Eq. (18) to obtain

$$c^\pm = c_0\exp(\mp\phi/\varsigma_T) \tag{19}$$

where c_0 denotes the concentration of both ions in the bulk, and

$$\varsigma_T = \frac{k_BT}{ze}$$

is the thermal potential. Here ϕ denotes the potential referred to the bulk potential. Eq. (19) is a kind of Boltzmann equation. We notice that $c^\pm\rightarrow c_0$ as $\phi\rightarrow 0$ in the bulk, and that when the surface is negatively charged ($c^+>c_0$ and $c^-<c_0$) the potential must be negative ($\phi<0$) in the EDL, and vice versa. To derive the expression for ϕ in terms of the coordinate n, we substitute (19) into (17) to have

$$\varepsilon\varepsilon_0\frac{\partial^2\phi}{\partial n^2} = 2c_0ze\sinh(\phi/\varsigma_T) \tag{20}$$

assuming that ε is constant. This can be integrated and the result is [3]

$$\phi = 4\varsigma_T \tanh^{-1}[\tanh(\varsigma/4\varsigma_T)\exp(-n/\lambda_D)] \quad (21)$$

where ς is the zeta potential, i.e. the potential evaluated at the interface n=0, and

$$\lambda_D = \sqrt{\frac{\varepsilon\varepsilon_0 k_B T}{2z^2 e^2 c_0}} \quad (22)$$

is the so called 'Debye screening length' representing the order of the EDL thickness; its inverse is usually written as $\kappa(\kappa=1/\lambda_D)$ and called 'Debye-Hückel parameter' [3]. When the zeta potential is much less than the thermal potential, i.e. $\varsigma \ll \varsigma_T$, then (21) becomes simply

$$\phi = \varsigma \exp(-n/\lambda_D) \quad (23)$$

The areal charge density (charge per unit area of the surface within EDL) σ_D [C/m^2] can be obtained from

$$\sigma_D = \int_0^\infty \rho_e dn \quad (24)$$

Substituting (17) into (24) and considering (21) gives

$$\sigma_D = -4zec_0\lambda_D \sinh(\varsigma/2\varsigma_T) \quad (25)$$

Sometimes it will be useful to define the differential capacitance of the diffuse layer C_D as follows [3].

$$C_D = \frac{d\sigma_D}{d\varsigma} = \frac{\varepsilon\varepsilon_0}{\lambda_D}\cosh(\varsigma/2\varsigma_T) \quad (26)$$
$$= 228.5z\sqrt{c_0}\cosh(19.46z\varsigma)$$

where the numerical values are for water at 25 [^{o}C] with c_0 in [mol/l] or [M], ς in [V] and C_D in [μF/cm^2]. Eq. (26) is useful in the prediction of the zeta potential from the experimental measurement of the EDL capacitance.

5.2. Electric Multiple Layer under AC

It was shown from the asymptotic analysis of Suh & Kang [4] that the region near the surface of an electrode under AC with angular frequency ω, the frequency being $f=\omega/2\pi$, can be split into three (for the steady state) or four (for the transient state) layers as shown in Fig. 8. The innermost, thinnest layer is 'Stern layer' devoid of ions. The next layer called 'inner layer' corresponds to the 'diffuse layer' in the classical EDL structure. In this layer, the time

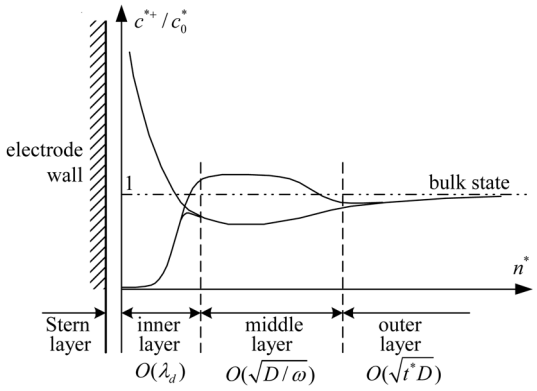

Fig. 8. Four-layer structure near an electrode wall under AC (from Suh & Kang [4]).

scale is very small, i.e. ions respond to the change of the potential on the electrode surface very quickly. So, this layer is governed by the steady-state equation like (18), and so the Boltzmann distribution (19) holds. As shown in Fig. 8, thickness of this layer, i.e. the Debye length, is independent of the frequency of the external AC. The next layer is called 'middle layer' governed by

$$\frac{\partial c^{\pm}}{\partial t} = D\nabla^2 c^{\pm} \quad (27)$$

implying that the conduction term is negligible. This does not necessarily mean that the conductive transport is absent in this layer. In fact, in this layer the conductive flux of ions is in the same order of magnitude as the diffusive flux, but its magnitude is almost constant across the middle layer so that its divergence $\nabla \cdot \mathbf{J}_i^C$ vanishes. It was found that thickness of the middle layer is of $O(\sqrt{D/\omega})$ as indicated in Fig. 8. The outermost layer called 'outer layer' is characterized by a very slow diffusion process. Here again the governing equation is the same as (27), but the effective time scale is much larger than that of the middle layer $O(1/\omega)$.

The asymptotic solutions of the ion transport equation (12) in each of these layers have been obtained by e.g. Suh & Kang [4]. In deriving the solutions they employed an adsorption model, in which ions are assumed to be adsorbed at the edge of the Stern layer, and a Stern-layer model, in which it is assumed that there exist no ions in the Stern layer. From the second assumption, we can set the RHS of Eq. (17) zero, and immediately we

derive the fact that the potential distribution within the Stern layer is linear. So, we can write

$$\left(\frac{\partial\phi}{\partial n}\right)_{0-} = \frac{\phi_0 - V_{00}\cos\omega t}{\lambda_s} \tag{28}$$

where ϕ_0 denotes the value of ϕ at n=0 (interface between the Stern and inner layers), V_{00} the amplitude of the external potential and λ_s the Stern-layer thickness. LHS of (28) denotes the slope of ϕ at the point very close to the interface n=0 to the Stern-layer side; this slope is constant across the Stern layer. Next, we integrate the Poisson equation (17) over a very thin interface from n=0$^-$ to n=0$^+$, where the cations and anions are supposed to be adsorbed as much as Γ^+ and Γ^- respectively per unit area following our adsorption model. The result is

$$\varepsilon\varepsilon_0\left(\frac{\partial\phi}{\partial n}\right)_{0+} - \varepsilon_S\varepsilon_0\left(\frac{\partial\phi}{\partial n}\right)_{0-} = -\sigma_a \tag{29}$$

where ε_S denotes the dielectric constant of the Stern layer and

$$\sigma_a = ze(\Gamma^+ - \Gamma^-)$$

is the surface charge density caused by the ion adsorption at the interface. Then, we obtain the following equation for the potential at the interface between the Stern and inner layers.

$$\phi_0 = V_{00}\cos\omega t + \lambda_{Seff}\left(\frac{\partial\phi}{\partial n}\right)_0 + \lambda_{Seff}\sigma_d/(\varepsilon\varepsilon_0)\,, \tag{30}$$

where λ_{Seff} represents the effective thickness of the Stern layer; $\lambda_{Seff}=\lambda_S\varepsilon/\varepsilon_S$.

On the other hand we must specify the relation between the adsorptions $\Gamma^\pm$ and the concentrations $c^\pm$ at n=0. For this we can use an isotherm such as the Langmuir type

$$\Gamma^\pm = \frac{\Gamma_{max}\alpha c_0^\pm}{1+\alpha(c_0^+ + c_0^-)} \tag{31}$$

where Γ_{max} is the limit value of $\Gamma^\pm$ available at $c_0^\pm \to \infty$; this magnitude should be proportional to a^{-2}. Further, the parameter α controls the rate of increase of $\Gamma^\pm$ upon change of $c_0^\pm$ in the limit $c_0^\pm \to 0$. Fig. 9 is a typical example of the numerical results for the effect of the adsorption on the potential distribution within the Stern and inner layers. We see that although the slope of the potential ϕ in the Stern layer is almost independent of the adsorption parameters, the potential drop across the inner layer (i.e. zeta potential) decreases significantly with the adsorption effect.

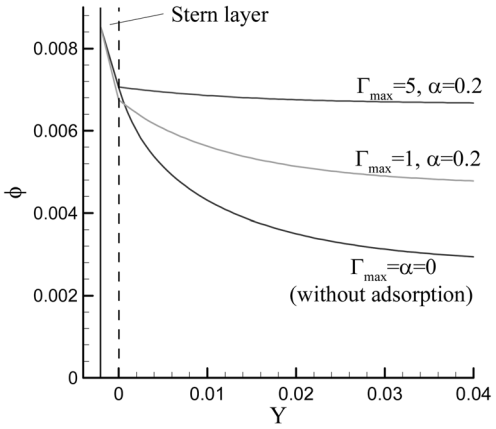

Fig. 9. A typical numerical result for the distribution of potential in the Stern and inner layers with various non-dimensional-parameter settings [4]. Here, all the variables are dimensionless; e.g. Γ and α correspond to Γ'_{max} and α' respectively in the text.

We finally need a dynamical equation that relates what happening in the electrical layers and the potential field in the bulk. Fortunately the middle layer does not give any significant effect in such relationship as far as the applied potential remains small, that is, in the weakly non-linear regime; when the applied voltage is high enough, it happens that the middle layer is devoid of ions, at least temporally, so that the asymptotic solutions provided by Suh and Kang [4] should be modified. Here we just present the basic dynamical equations needed to supply the boundary conditions for solving the Laplace equation

$$\nabla^2\phi = 0 \tag{32}$$

for the bulk. The boundary conditions can be presented in terms of the dimensionless areal charge density q determined by the dynamical equation

$$\frac{dq}{dt} = \frac{\sqrt{2}\,\omega\lambda_{dif}}{(1+\beta)\varsigma_T}\left(\frac{\partial\phi}{\partial n}\right)_w \tag{33}$$

where the subscript 'w' indicates evaluation at the wall n=0 from the solution of Eq. (32), $\lambda_{dif} = \sqrt{D/\omega}$

represents the middle-layer thickness and β is a dimensionless parameter defined as

$$\beta = \frac{8\Gamma'_{max}\alpha'\sqrt{\gamma}(8+16\alpha'+\gamma q^2)}{\sqrt{16+\gamma q^2}(4+8\alpha'+\alpha'\gamma q^2)} \tag{34}$$

Here the dimensionless parameter $\gamma=(\lambda_{dif}/\lambda_D)^2/2$ is usually large. Further, Γ'_{max} and α' are dimensionless parameters related to Γ_{max} and α as follows.

$$\Gamma'_{max} = \frac{\sqrt{2}\Gamma_{max}}{c_0\lambda_{dif}}, \quad \alpha' = c_0\alpha \tag{35}$$

Eq. (33) has been derived by subtracting the equation for c^- from that for c^+ (those are shown in Eq. (12)) and integrating the result over the inner layer. The effect of the adsorption has been considered through the factor β; note that β=0 when no adsorption occurs. Then the potential at the wall surface is calculated from

$$\phi_w = V_{00}\cos\omega t + \left(\frac{\gamma\varsigma_T\lambda_{Seff}}{\sqrt{2}\lambda_{diff}}\right)q - \varsigma_T\ln\left(\frac{\sqrt{16/\gamma+q^2}-q}{\sqrt{16/\gamma+q^2}+q}\right) + \left(\frac{\lambda_{Seff}}{\varepsilon\varepsilon_0}\right)\sigma_a \tag{36}$$

where σ_a is directly calculated with

$$\sigma_a = \frac{\Gamma_{max}ze\alpha c_0\gamma q\sqrt{16/\gamma+q^2}}{4+8\alpha c_0+\alpha c_0\gamma q^2} \tag{37}$$

The zeta potential becomes

$$\phi_0 - \phi_w = \varsigma_T\ln\left(\frac{\sqrt{16/\gamma+q^2}-q}{\sqrt{16/\gamma+q^2}+q}\right) \tag{38}$$

The numerical procedure can be described as follows.

(i) Solve (32) for ϕ over the whole fluid region with the boundary value ϕ_w.

(ii) Get the gradient $(\partial\phi/\partial n)_w$ and update q by using (33).

(iii) Then calculate ϕ_w by using (36).

(iv) Increase the time level and repeat (i)-(iii).

For more detailed description on derivation of the above formulas, refer to the paper by Suh & Kang [4]. Fig. 10 demonstrates the numerical procedure.

6. Slip Velocity and Driven Flow - Electroosmosis

Since the electrical layer is very thin in microfluidic flows, we can neglect the tangential variation of the variables in the momentum equations when compared with the normal variation. We can also neglect the transient and convective terms in most applications. Then we can write Eq. (15) in the component forms as follows.

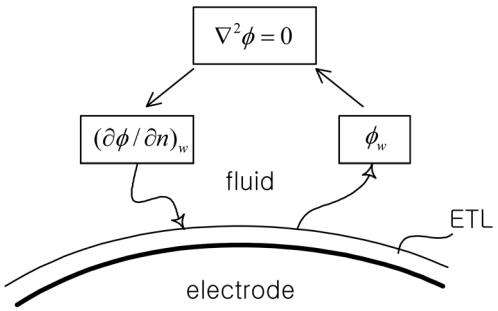

Fig. 10. Schematic illustrating the numerical procedure for obtaining the potential distribution in the bulk of the electrolyte contacting the electrode under AC, where the ETL (electric triple layer) effect has been modeled by the asymptotic solutions.

$$\frac{\partial^2 u}{\partial n^2} = \frac{1}{\eta}\frac{\partial p}{\partial s} - \frac{\varepsilon\varepsilon_0}{\eta}\frac{\partial^2\phi}{\partial n^2}\frac{\partial\phi}{\partial s} \tag{39a}$$

$$0 = \frac{1}{\eta}\frac{\partial p}{\partial n} - \frac{\varepsilon\varepsilon_0}{\eta}\frac{\partial^2\phi}{\partial n^2}\frac{\partial\phi}{\partial n} \tag{39b}$$

where u represents the velocity component along the s-direction. We can integrate Eq. (39b) immediately to obtain

$$p(s,n) = \frac{\varepsilon\varepsilon_0}{2}\left(\frac{\partial\phi}{\partial n}\right)^2 + P(s) \tag{40}$$

where the function $P(s)$ is independent of the potential ϕ; this pressure should act as a driving term for the case of pressure driven flows. Since we are interested in the electrically induced flow we can set $P(s)$=0 without loss of generality. We also note the pressure built in the inner layer should be always higher than that of the other layers because $\partial\phi/\partial n$ in the inner layer is much larger than that of the other layers; the excess pressure corresponds to the 'osmotic pressure'. Differentiating (39) w.r.t. s and substituting the result into (39a), we get

$$\frac{\partial^2 u}{\partial n^2} = \frac{\varepsilon\varepsilon_0}{\eta}\left(-\frac{\partial^2\phi}{\partial n^2}\frac{\partial\phi}{\partial s} + \frac{\partial\phi}{\partial n}\frac{\partial^2\phi}{\partial s^2}\right) \tag{41}$$

Now we apply the asymptotic solutions of ϕ to Eq. (41) and after some algebra we arrive at the following formula for the *instantaneous* slip velocity at the surface.

$$u_w = \frac{\varepsilon\varepsilon_0}{\eta}(\phi_0 - \phi_w)\left(\frac{\partial\phi}{\partial s}\right)_w \tag{42}$$

where the zeta potential $(\phi_0-\phi_w)$ is calculated from (38) and ϕ_w needed for $(\partial\phi/\partial s)_w$ from (36). The slip velocity to be used as the boundary condition in the flow-field calculation is then given by the time average of Eq. (42);

$$u_{slip} = \frac{\varepsilon\varepsilon_0}{\eta}\langle(\phi_0 - \phi_w)(\partial\phi/\partial s)_w\rangle \tag{43}$$

where $\langle\ \rangle$ denotes the time average over one cycle of AC. We see that Eq. (43) corresponds to the Smoluchowski's slip-velocity formula for the case of AC [3].

The viscous flow of the bulk fluid driven by the slip velocity on the electrode walls, which is called 'electro-osmotic flow', can be calculated by using a standard CFD technique if the slip velocity has been set up. As a typical problem, a rectangular cavity having a pair of coplanar electrodes on the bottom boundary has been investigated as shown in Fig. 11. This has been studied experimentally by Green et al. [5] and they provided the experimentally measured data for the slip velocity on the electrode surfaces as shown by symbols in Fig. 12. The electrodes were 250 [μm] long and separated by 25 [μm]. Alternating current with V_{00}=0.25 [V] was applied. The concentration of the KCl electrolyte was set at 0.141 [mM] equivalent to c_0=0.85×10^{23} [/m^3], the diffusivity being D=1.92×10^{-9} [m^2/s]. The Debye screening length is calculated to be λ_D=25.4 [nm] and the thermal potential ς_T = 25 [mV]. Fig. 12 compares the theoretical/numerical results and the experimentally measured ones. It shows that without the adsorption effect the experi-

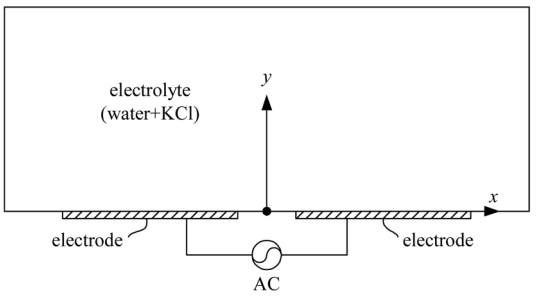

Fig. 11. Geometry of the ion-transport and subsequent momentum-transport problem around a pair of coplanar electrodes under AC.

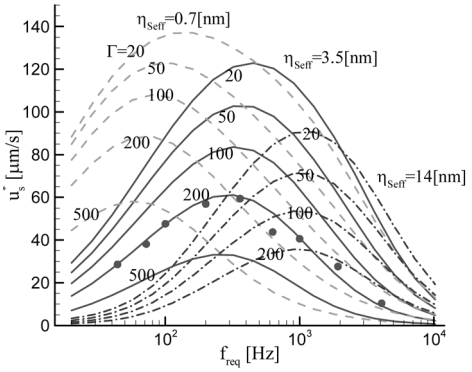

Fig. 12. Parameter tuning for matching the slip-velocity data obtained from the theory considering the adsorption effect (solid lines) and that of the experiment (symbols) obtained by Green et al. [5] for the case of electrolyte "A". Here, the parameter Γ is dimensionless; that is, this corresponds to Γ'_{max} in the text. Dash-dot and dashed lines are the theoretical/numerical results without adsorption.

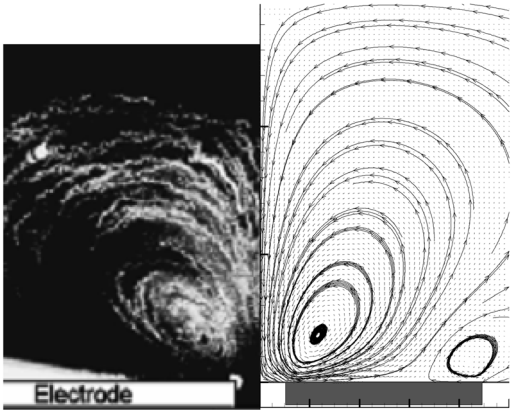

Fig. 13. Streamlines of the electro-osmotic flow driven by the slip velocity on the electrodes under AC measured from the experiment (LHS) by Green et al. [5] and that obtained from the theoretical/numerical method (RHS) for the case of electrolyte "A" with the external potential amplitude at 0.25 [V] and the frequency at 100 [Hz].

mental results cannot be matched accurately. On the other hand, for a suitable parameter setting the measured data can be well fitted by the asymptotic solutions. Fig. 13 shows an example of flow field calculated from the theoretical/numerical work in comparison with the experimental observation of Green et al. [5]. It shows good agreement although the observed flow pattern near the electrodes' outer edges is not clear. Further analysis should be needed for instance as to enlarging the applicability of the present model.

7. Visulization of Ion Motions

7.1 Velocity Field

Most of the studies on the ion transport have been done in terms of its primary influence on the fluid flows, that is the electroosmotic flows. So the motion of ions has naturally been put aside from our interests. On the other hand, in order to shorten the gap between the theoretical/numerical solutions and the experimental results, we may have to consider the kinematics of ions so that it can lead to improved models.

We have derived the Nernst-Planck equation like (11) or (12). On the other hand the conservation of ions implies the following equation.

$$\frac{\partial c_i}{\partial t} + \nabla \cdot (\mathbf{u}_i c_i) = 0 \tag{44}$$

Comparing this with (12), where the advection term is to be neglected, we can derive the velocity vector of the ion motion as follows.

$$\mathbf{u}_i = -D_i \left[\nabla \ln c_i + \left(\frac{z_i e}{k_B T} \right) \nabla \phi \right] \tag{45}$$

This indicates that the velocity field can be written as $\mathbf{u}_i = \nabla \varphi_i$ where φ_i denotes the velocity potential to be given by

$$\varphi_i = -D_i \left[\ln c_i + \left(\frac{z_i e}{k_B T} \right) \phi \right] \tag{46}$$

For instance, in the bulk we have $c_i \cong c_0 = \text{constant}$, so the first term within [ ] on RHS of (46) becomes very small and the velocity potential is proportional to the electric potential. Furthermore the divergence of the velocity vector, $\nabla \cdot \mathbf{u}_i$, also vanishes in the bulk because the Laplace equation (32) must apply there.

For the 2-D case we can decompose the velocity vector as $\mathbf{u}_i = u_i \mathbf{e}_s + v_i \mathbf{e}_n$, where $\mathbf{e}_s$ and $\mathbf{e}_n$ are unit vectors along the tangential and normal directions, respectively, with respect to the electrode surface. Then (44) becomes

$$\frac{\partial c_i}{\partial t} + \frac{\partial u_i c_i}{\partial s} + \frac{\partial v_i c_i}{\partial n} = 0 \tag{47}$$

Usually the second term is very small compared with the third one. Then we are left with

$$\frac{\partial c_i}{\partial t} + \frac{\partial v_i c_i}{\partial n} = 0 \tag{48}$$

This equation can be used in determining the normal component of the velocity within the electric layer as follows.

$$v_i = \frac{1}{c_i} \int_{\infty}^{n} \frac{\partial c_i}{\partial t} dn + v_{i\infty} \tag{49}$$

where

$$v_{i\infty} = -\text{sign}(z_i) \frac{D}{\varsigma_T} \left(\frac{\partial \phi}{\partial n} \right)_{\text{wall}} \tag{50}$$

is the normal velocity calculated from the solution of (32) evaluated at the electrode surface. When the adsorption effect were not existent, v_i should tends to zero when the electrode surface is approached. The order of magnitude of $v_{i\infty}$ for the case of facing electrodes with the standard set-up of Suh and Kang [4] was found to be $v_{i\infty}$=190 [μm/s]. The distance traveled by the ion at 100 [Hz] is then computed to be 0.32 [μm]. Further, the thickness of the inner and middle layer is approximately 0.24 [μm] and 4.8 [μm], respectively. This indicates that the travel distance of the ions is in the same order of magnitude as that of the electric-layer thickness. However, the ion's travel distance becomes decreased as the frequency is increased. For instance at 10,000 [Hz] it reaches down to 0.0032 [μm], which is very small compared even with the inner-layer thickness, that is independent of the AC frequency.

On the other hand, determining u_i, the tangential component of the velocity, has not been clearly defined. Since the gradient of the ion concentration along the tangential direction is usually much

smaller than that along the normal direction, the contribution of the ion concentration to its motion may be neglected compared to the conduction effect. So, we are allowed to assume the followings.

$$u_i = -\text{sign}(z_i)\frac{D}{\zeta_T}\left(\frac{\partial \phi}{\partial s}\right) \tag{51}$$

We have conducted interactive numerical computations of the Laplace equation (32) and the dynamical equation (33) for the model shown in Fig. 11 to obtain the velocity field during one period of AC. After the potential becomes periodic (usually after 10 periods), we assume that the velocity data can be expanded in Fourier series as follows.

$$u = \sum_{k=1}^{\infty}(a_{uk}\cos kt + b_{uk}\sin kt) \tag{52a}$$

$$v = \sum_{k=1}^{\infty}(a_{vk}\cos kt + b_{vk}\sin kt) \tag{52b}$$

where the velocity data are calculated by using (51) for u and (50) for v. We obtain the Fourier coefficients a_{uk}, b_{uk}, a_{vk} and b_{vk} at each grid point in the numerical domain. These coefficients can be considered as functions of spatial variables. It turns out that only with 20 harmonics, (52a) and (52b) can reproduce the numerical data very accurately. Fig. 14(a) shows the typical evolution of the cation's velocity vector at the point 5 [μm] distant from the leading edge of one of the electrode pair under AC. The data in Fig. 14 are obtained from the asymptotic solutions provided by Suh and Kang [4]. The bulk pattern shows almost completely symmetric pattern whereas the middle-layer pattern exhibits significantly asymmetric one. This is of course caused by the asymmetric distribution of concentration in each half period. The velocity data for the inner layer (though not shown in this paper) on the other hand give not only asymmetric pattern but also significantly large magnitude of v, which is of course not physically relevant. Determining the normal component of the velocity vector by using (49) is in fact expected to produce large errors, because the asymptotic solutions are obtained from the quasi-steady-state assumption for the inner layer. Thus we may have to develop a new model when more accurate picture for the ion motions is required in the electric layer. In this lecture therefore we focus our attention on the bulk region only. On the other hand Fig. 14(b) illustrates the significant influence of the external potential on the velocity magnitude.

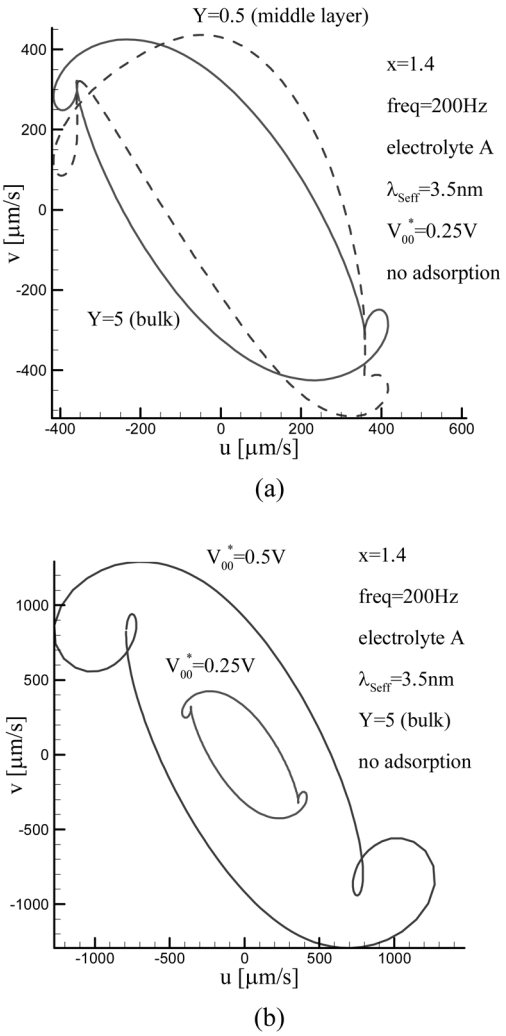

Fig. 14. Typical evolutions of the cation velocity vector for the case of electrolyte "A" with the frequency at 200 [Hz]. Plot (a) shows difference of the velocity vector in the bulk and middle layers (here the measurement position is at 5 [μm] away from the leading edge of the electrode). Plot (b) shows the dependence of the velocity magnitude on the external potential.

7.2. Motional Trajectory

We have seen that the velocity vectors are completely periodic. More precisely, after one period of AC the velocity vector returns back to the initial value as shown in Fig. 14. However this does not necessarily mean that the same argument holds for the trajectory of ion motion. In another words, after one period, the ion can be shifted from the initial position. So, after many periods the ion can travel a long distance and arrive at the place far away from the initial position. This phenomenon is well known in the fluid mechanics and called Stokes' drift motion. The ion's trajectory can be obtained from the time integration of the following equations.

$$\frac{dx}{dt} = \tilde{\varepsilon} u, \quad \frac{dy}{dt} = \tilde{\varepsilon} v \tag{53}$$

where now all the variables are dimensionless and $\tilde{\varepsilon} = \varepsilon_1^2$ is a small parameter. The dimensionless velocity vector components are related to the dimensionless potential as follows.

$$u = -\gamma \frac{\partial \phi}{\partial x}, \quad v = -\gamma \frac{\partial \phi}{\partial y} \tag{54}$$

Fig. 15 shows typical plots of the cation's trajectory with the external potential amplitude at 0.5 [V] and the other parameters being fixed the same as in Fig. 14. First, we note that the shape of the trajectory during one period is not the same as that of the velocity vector; compare Fig. 15(a) with a larger loop in Fig. 14(b). As will be shown shortly this means that the higher harmonic terms have important contribution to the ion motions. Next, we see that the drift motion is downward in Fig. 15(a) while it is upward in Fig. 15(b); the former represents the behavior of cation motion near the electrode surface and the latter in the region between the electrode pair.

The Stokes' drift velocity can be obtained by applying a perturbation technique to the equations of motion (53). For this we assume

$$x = x_0 + \tilde{\varepsilon} x_1(t) + \tilde{\varepsilon}^2 x_2(t) + \ldots$$
$$y = y_0 + \tilde{\varepsilon} y_1(t) + \tilde{\varepsilon}^2 y_2(t) + \ldots$$

We then substitute these into (53), where the velocity vector is expanded like

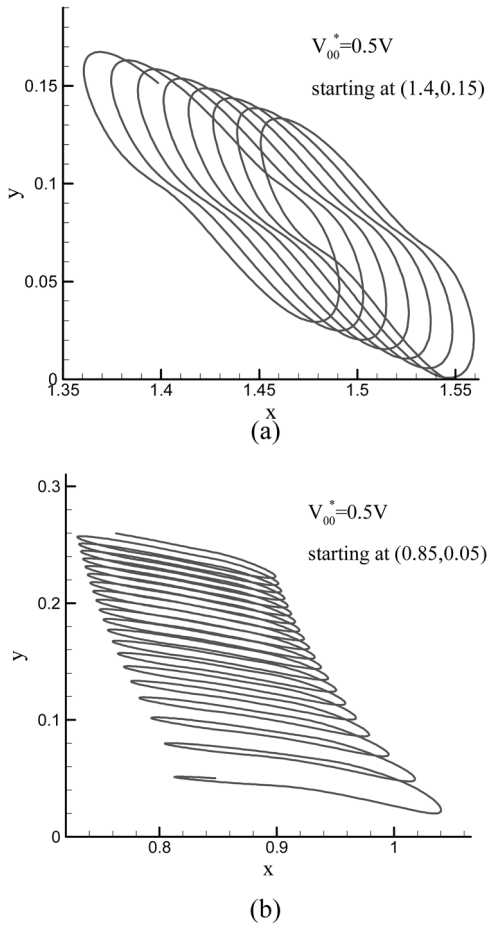

Fig. 15. Typical cation trajectories for the case of electrolyte "A" with the external potential amplitude at 0.5 [V] and the frequency at 200 [Hz]. Particle starts at (a) (1.4, 0.15) and (b) (0.85, 0.05). All the other parameters are the same as in Fig. 14.

$$u = u(x_0, y_0, t) + \tilde{\varepsilon}\left(\frac{\partial u}{\partial x}\right)_0 (x - x_0) + \tilde{\varepsilon}\left(\frac{\partial u}{\partial y}\right)_0 (y - y_0) \ldots \tag{55a}$$

$$v = v(x_0, y_0, t) + \tilde{\varepsilon}\left(\frac{\partial v}{\partial x}\right)_0 (x - x_0) + \tilde{\varepsilon}\left(\frac{\partial v}{\partial y}\right)_0 (y - y_0) \ldots \tag{55b}$$

collect the terms in the same power of $\tilde{\varepsilon}$ and obtain a series of equations. The leading-order equations, in $O(\tilde{\varepsilon})$, take the following form.

$$\frac{dx_1}{dt} = \sum_{k=1}^{\infty} (a_{uk0} \cos kt + b_{uk0} \sin kt)$$

$$\frac{dy_1}{dt} = \sum_{k=1}^{\infty}(a_{vk0}\cos kt + b_{vk0}\sin kt)$$

where the Fourier coefficients are to be evaluated at the reference point (x_0, y_0). Integration of these w.r.t. time gives

$$x_1 = \sum_{k=1}^{\infty}\frac{1}{k}(a_{uk0}\sin kt - b_{uk0}\cos kt) \tag{56a}$$

$$y_1 = \sum_{k=1}^{\infty}\frac{1}{k}(a_{vk0}\sin kt - b_{vk0}\cos kt) \tag{56b}$$

This set of coordinates represents the primary trajectory of the ion motion. Let us compare these with the velocity components (52a) and (52b). For instance, if the fundamental harmonic (i.e. the term with k=1) is dominant and all the higher harmonics can be neglected, the displacement vector (x_1, y_1) should give the trajectory in the same shape as that of the velocity vector (u, v) evaluated at the reference point; the phase of the displacement is of course behind that of the velocity as much as a quarter period. On the other hand if the higher harmonics become more important, then those shapes may be quite different from each other, as shown in Fig. 14(b) and Fig. 15(a). Next we substitute (56a) and (56b) to the system of higher-order equations in $O(\tilde{\varepsilon}^2)$. The solutions can be decomposed into the steady and unsteady parts. It can be shown that the steady parts are

$$u_{2D} \equiv \langle \frac{dx_2}{dt} \rangle = \sum_{k=1}^{\infty}\frac{1}{2k}\frac{\partial}{\partial y}(a_{vk}b_{uk} - a_{uk}b_{vk}) \tag{57a}$$

$$v_{2D} \equiv \langle \frac{dy_2}{dt} \rangle = \sum_{k=1}^{\infty}\frac{1}{2k}\frac{\partial}{\partial x}(a_{uk}b_{vk} - a_{vk}b_{uk}) \tag{57b}$$

which represent the Stokes' drift velocity components. Here again we can confirm the divergence-free property of the drift-velocity vector, i.e. $\nabla \cdot \mathbf{u}_{2D} = 0$. Further we can derive the stream function as follows.

$$\psi_{2D} = \sum_{k=1}^{\infty}\frac{1}{2k}(a_{vk}b_{uk} - a_{uk}b_{vk})$$

We can address a few comments regarding the

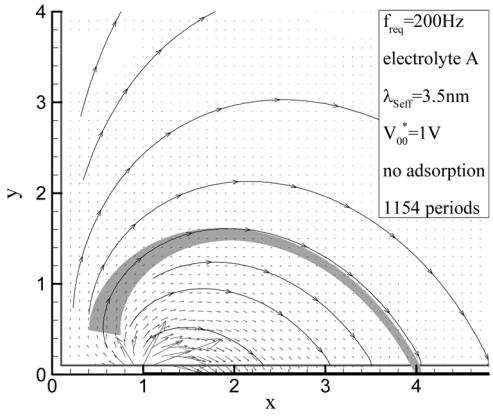

(a)

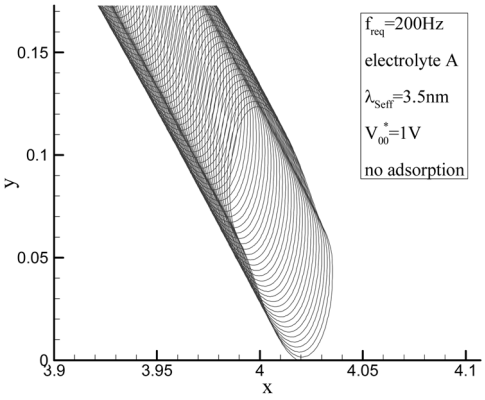

(b)

Fig. 16. Stokes' drift velocity field computed by using (57a) and (57b) the results being shown as vector plots in (a). Also shown in this plot are some of the streamlines constructed from the field. In (a) a typical trajectory of a cation having started at the point (0.5, 0.5) is also shown. Plot (b) shows a magnified view of the trajectory near the electrode surface. Parametric values used in this visualization are shown in the figure.

Stokes' drift velocity. First, we notice that when the velocity field is spatially uniform the Stokes' drift velocity vanishes because the coefficient functions are constant. This can occur even when the trajectory is elliptic, i.e. not linear. Next, when $a_{vk}b_{uk} - a_{uk}b_{vk}$=0 for every k, no Stokes' drift motion can be expected either. This corresponds to the case when the two velocity components u and v have the same

phase. In the (u,v) space this describes, in general, a curved line. For the anion's case the primary velocity is reversed as can be seen from Eqs. (50) and (51). Therefore the velocity has phase difference as much as half period, but both ions have the same rotational direction in the (u,v) space; this means that when the cation moves up, the anion moves down, and when the cation moves to the left, the anion moves to the right, etc. Then we expect that the Stokes' drift motion should have the same direction for both ions. This can be understood from (57a) and (57b); if the coefficients change their signs altogether, u_{2D} and v_{2D} keep their signs.

Fig. 16(a) shows the Stokes' drift velocity vector plot obtained by using (57a) and (57b). It reveals that velocity field is strongest near the electrode edge, situated at x=1. It also shows that the cations and anions should accumulate on the electrode surface whereas they become scarce in the region between the pair of electrodes.

7.3. Further Discussions

The Stokes' drift motion is not temporary but persistent as far as the asymptotic solutions provided by Suh and Kang [4] is correct. On the other hand, abundance and scarceness of such ions in differentiated spaces may give rise to concentration gradient. Then we can conjecture that diffusion caused by the non-zero concentration gradient may block the Stokes' drift motion. If this scenario is true, then we expect again the non-zero build-up of charge in the corresponding space. This charge in turn will affect the ion motion again. We are curious if such scenario may be relevant, if the subsequent effect can be formulated effectively and if the effect may be significant in determining the electroosmotic flows. This issue is left as our future study.

Acknowledgment

This work was supported by the Korea Science and Engineering Foundation (KOSEF) through the National Research Laboratory Program funded by the Ministry of Science and Technology (No. 2005-1091).

References

1) Tabeling, P., 2005, *Introduction to Microfluidics*, Oxford University Press.
2) Lyklema, J., 1995, *Fundamentals of Interface and Colloid Science*-Vol. II, Academic Press.
3) Hunter, R.J., 2001, *Foundations of Colloid Science*, Oxford University Press.
4) Suh, Y.K. and Kang, S., 2008, "Asymptotic analysis of ion transport in a nonlinear regime around polarized electrodes under ac", *Phy. Rev.* E **77**, 031504.
5) Green, N.G., Ramos, A., Gonzalez, A., Morgan, H. and Castellanos, A., 2002, "Fluid flow induced by nonuniform ac electric fields in electrolytes on microelectrodes. III. Observation of streamlines and numerical simulation", *Phys. Rev.* E **66**, L25.